crystals

MDPI

Article

Investigation of Hafnium Oxide Containing Zirconium in the Scaled Region on the Surface of As-Cast Nickel-Based Single Crystal Superalloy Turbine Blades

KeeHyun Park * and Paul Withey

School of Metallurgy and Materials, University of Birmingham, Birmingham B15 2TT, UK
* Correspondence: k.park.2@bham.ac.uk

Abstract: Surface scale is usually formed in the aerofoil part of as-cast nickel-based single crystal turbine blades by the strong interaction between the mould wall and the melt, and the subsequent oxidation of the fresh metallic surface of the casting. For better understanding of the scaling, the scaled region was investigated, and an interesting region containing hafnium oxides and a rhenium-rich particle was found. Generally, a continuous aluminium oxide layer was detected on the outer surface of the base material and covered the surface of an unscaled region. In contrast, there was no oxide on the surface of a scaled region, but it was replaced by several tiny particles remaining locally on the outer surface of the base material. SEM-EDX and TEM-EDX point analysis of these particles indicated not only the existence of high amounts of hafnium, but also several particles such as hafnium oxide, aluminium oxide, and even tiny metallic particles. Most of all, STEM-EDX point analysis clearly detected zirconium in the hafnium oxide. Furthermore, a rhenium-rich particle was also detected towards the outer surface of the base material, which suggested that the surface of the scaled region might be exposed to high enough temperatures to allow the diffusion of heavy alloying elements. Based on the observation, the formation mechanism of hafnium oxide containing zirconium and its meaning was discussed.

Keywords: superalloys; turbine blade; surface scale; hafnium oxide; zirconium

check for updates

Citation: Park, K.; Withey, P. Investigation of Hafnium Oxide Containing Zirconium in the Scaled Region on the Surface of As-Cast Nickel-Based Single Crystal Superalloy Turbine Blades. *Crystals* **2023**, *13*, 277. https://doi.org/10.3390/cryst13020277

Academic Editors: Pascal Thome, Markus Stricker, Jan Frenzel and Umberto Prisco

Received: 9 December 2022
Revised: 26 January 2023
Accepted: 1 February 2023
Published: 6 February 2023

Copyright: © 2023 by the authors. Licensee MDPI, Basel, Switzerland. This article is an open access article distributed under the terms and conditions of the Creative Commons Attribution (CC BY) license (https://creativecommons.org/licenses/by/4.0/).

1. Introduction

Nickel-based single crystal superalloys which are one of the most advanced engineering materials have been used to manufacture turbine blades for gas turbine engines for aerospace and power generation. Within the gas turbine engine, nickel-based superalloys are used for components in high-pressure and low-pressure turbines. Of these, the high pressure turbine proves to be the most challenging of environments with gas stream temperatures above the melting point of the superalloys and component loads of many tonnes due to the rotational speeds [1]. As a result, high pressure turbine blades should survive the operating temperature under severe loading conditions through the deployment of nickel-based single crystal superalloys. When turbine blades were first developed, they had equiaxed crystal structure. As casting methods developed, columnar microstructures were produced and finally, monocrystalline superalloys were produced [1–3]. The single crystal turbine blade gives the opportunity for improved fatigue life or increased temperature use, a robust heat treatment, and significantly, the removal of some elements such as boron and carbon which had been added for grain boundary strengthening [1–3]. Even though there is a possibility that in the future the low-pressure turbine parts can be manufactured by additive manufacturing methods, the high-pressure turbine blades are currently manufactured just by an investment casting process which allows complex shapes, internal cooling passages, and significantly eliminates grain boundaries.

Nickel-based single crystal superalloy turbine blades manufactured by this investment casting process have superior mechanical strength and surface stability at high temperatures

mainly due to two different hardening mechanisms: precipitation hardening and solid solutioning hardening. Multiple steps of melting, casting, and heat treatment processing of turbine blades induce precipitation hardening by a relatively uniform precipitation of high volume fractions (approximately 70%) of an ordered γ' phase (Ni_3(Al, Ta, Ti)) in the face-centered cubic structure matrix (γ phase) which is stable from room temperature to the melting temperature [1]. Most of the turbine blade alloys contain a number of soluble elements such as cobalt, chromium, molybdenum, tungsten and rhenium which can induce solid-solutioning hardening to inhibit dislocation movement, to provide strong lattice cohesion, to reduce diffusion, and to decrease the stacking fault energy [1–4]. Furthermore, some minor elements such as niobium and hafnium are also added. Niobium has some effects on nickel-based alloys, such as solid solution hardening, large increase in γ' volume fraction and precipitation of γ'' or δ-Ni_3Nb, and hafnium has been *traditionally* added to improve the creep strength and ductility by strengthening grain boundaries and the adherence of the protective oxide layer [2,5–7].

The investment casting process for nickel-based single crystal turbine blades is performed through steps of assembling wax models, dipping into ceramic slurries, removing the wax, baking the mould, pouring the molten superalloy, controlling the solidification, and removing the investment shell, which are well described in many literature papers [1,8]. For the majority of single crystal castings, the slurry is a silica sol containing a zirconium silicate flour and is the primary contact to the liquid metal during casting. However, it is known well that the strong interaction between the dried ceramic slurry and the liquid metal [9–11] often induces a defect on the surface of as-cast turbine blades, such as surface scale [8,12–15]. Figure 1 shows an as-cast turbine blade with surface scale on the aerofoil which is indicated by an arrow. The scale is easily recognised due to the colour difference on the surface, i.e., the silver colour on this blade. A recent study by the authors clearly showed that when the molten metal meets the slurry, an initial aluminium oxide is formed but detached from the base material during cooling. Then, the fresh surface of the base material is exposed and subsequent oxidation of the base metal causes surface scale [15]. In industrial processing, the surface defect is simply removed by abrasively blasting, grinding and etching after solution heat treatment, but other surface defects such as surface pits [16] are often found after the processing of turbine blades. Several previous studies showed some results on the scale based on the observation of the scaled region [8,15]. Nonetheless, the surface scale is still a common problem in industry.

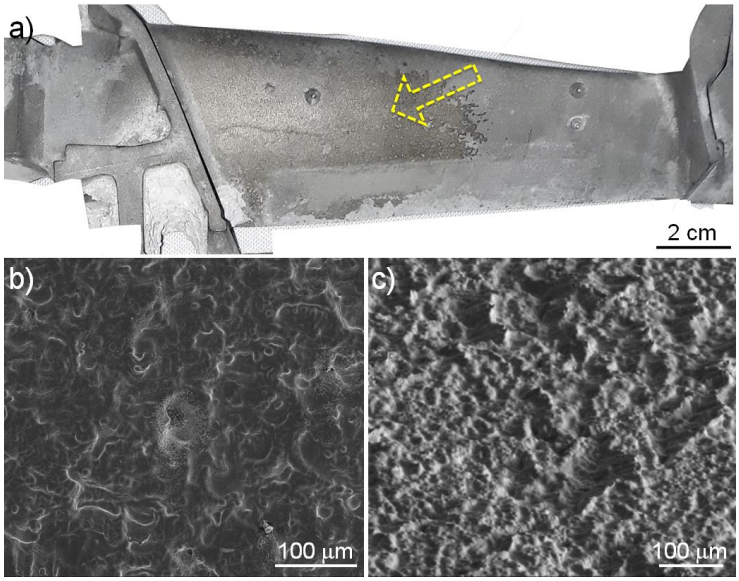


Figure 1. General images of surface scale: (**a**) silver-coloured surface scale in an as-cast turbine blade, and (**b**,**c**) low magnification SEM images acquired in the scaled region from a plain view (**b**) and a tilting view (**c**).

Thus, for a better understanding of the surface scale, the surface of a scaled region formed in a turbine blade has been observed in this study. A hafnium oxide containing zirconium as well as a rhenium-rich particle has been firstly detected near the top surface of a base material in the scaled region, which will support the formation mechanism of surface scale. Finally, even though hafnium is a minor alloying element in the third-generation nickel-based superalloy, this study will show that it may not be necessary to add the element because most of hafnium in the base material can be consumed by the formation of its oxide.

2. Experimental Section

2.1. Materials

A raw nickel-based superalloy (CMSX-10N) was used to manufacture single crystal turbine blades at an aerospace production manufacturing facility, Rolls-Royce plc, using an investment casting process. The composition of the raw superalloy is summarised in Table 1 and shows high amounts of refractory elements, in particular rhenium, but a negligible amount of hafnium. Casting was performed by directional solidification at nominally 1773 K (1500 °C), a vacuum level of a furnace chamber of approximately 10^{-6} atm and a withdrawal rate of approximately 5×10^{-5} m s^{-1}. The detailed investment casting process is described in Ref. [8]. Afterwards, the turbine blades containing the surface scale were removed from the runner system.

2.2. Microstructural Characterisation

The turbine blades containing the surface scale were cut by wire-guided electro discharge machining (EDM) and then ultrasonic-cleaned in ethanol for 5 min. The cut samples were observed using a high-resolution scanning electron microscope (field emission (FE)-SEM, FEI Quanta 3D dual beam FIB-SEM) equipped with an energy dispersive X-ray spectroscopy (EDX) system. The microscope was also used for cross-sectioning regions of interest by a focused ion beam (FIB) milling and thinning process. After SEM observation, TEM samples were made in the same chamber of the FIB machine by an in-situ FIB lift-out technique [17–21], and observed at an operation voltage of 200 kV using a transmission electron microscope (FE-TEM, FEI Tecnai F20) equipped with a scanning mode (STEM) and an EDX system.

For a basic chemical analysis, a SEM-EDX detector installed in the FIB machine was used. However, the superalloy (CMSX-10N) contains more than 10 alloying elements. Most of all, the close proximity of characteristic X-rays (M_α, keV), such as Hf (1.644), Ta (1.709), W (1.774), and Re (1.842) [22,23] resulted in the difficulty of clearly distinguishing each element in key areas. Therefore, the chemical analysis of these regions was performed by STEM-EDX with a nominal probe size of about 2 nm. For sufficient statistical confidence, compositions were acquired from more than 10 analysis areas and quantified by an analysis software (Oxford AZtecTEM) installed on the TEM. During TEM observation, TEM samples were cooled with liquid nitrogen to avoid or minimise microstructural changes in the irradiated area [18].

Table 1. Compositions (at %) of raw material, γ and γ′ phases measured in a fully heat-treated blade [24–26], the base material, hafnium oxide and aluminium oxide, and a Re-rich particle measured by STEM-EDX.

Element	Raw	Full Heat Treated		Base *	Hf Oxide	Al Oxide	Re-Rich
		γ	γ′				
Al	13.6	6.3	15.6	8.6	-	33.9	2.2
Ti	0.1	0.0	0.1	0.3	-	-	0.1
Cr	1.8	4.1	1.0	1.7	-	-	12.5
Co	3.2	5.9	2.7	3.1	-	-	4.7
Nb	0.0 **	0.0	0.0	0.0	-	-	0.5

Table 1. *Cont.*

Element	Raw	Full Heat Treated		Base *	Hf Oxide	Al Oxide	Re-Rich
		γ	γ′				
Mo	0.3	0.3	0.0	0.1	-	-	3.6
Hf	0.0 ***	0.0	0.0	0.1	36.7	-	0.1
Ta	3.0	3.6	4.6	4.6	-	-	1.2
W	1.9	3.4	2.4	0.9	-	-	7.6
Re	2.4	5.9	0.0	0.4	-	-	43.6
O	-	-	-	-	52.5	66.0	-
Zr	-	-	-	-	9.7	-	-
Ni	Bal.	Bal.	Bal.	Bal.	1.1	0.1	Bal.

* The 'Base' means the base material. **, *** The exact amounts of Nb and Hf are 0.04 and 0.001 at. pct, respectively.

3. Results

3.1. Formation of a Scaled Region and Detection of Particles Containing Hafnium

As shown in Figure 1, the surface scale is commonly found across the aerofoil adjacent to the platform region of a turbine blade. During casting, solidification progressed from right to left in Figure 1a; the region where the scale formed was towards the top of the casting and hence solidified last. SEM images acquired at low magnifications (Figure 1b,c) show that the surface of the scaled region is dimpled but no specific morphology is observed even after tilting of the region (Figure 1c). The microstructural observation of the scaled region itself is found elsewhere in detail [15].

SEM images acquired at higher magnifications within the scaled region (Figure 2), however, show an interesting microstructure. Figure 2a was acquired from the central region of Figure 1b within the scaled region. The general region in the silver-coloured surface scale shows a smooth and flat terrain of steps slightly protruding from the surface (Figure 2b), which is in good agreement with a previous study [15]. SEM-EDX point analysis was performed on the general surface and shown in Figure 3a. As expected, strong nickel, chromium, and aluminium peaks were detected. Even after cross-sectioning near the central region of Figure 2b by FIB milling after a protective platinum layer was deposited, there is no notable layer or particle on the top surface of the general scaled region (Figure 2c). However, some extraordinary microstructures were locally observed as shown in Figure 2d. A representative SEM-EDX spectrum of the region (shown in Figure 3b) indicated that the unusual microstructure was due to an aluminium oxide formed on the surface of cast components. It should be emphasised that during the SEM point analysis of the remaining aluminium oxide in the scaled region in Figure 2d, additional peaks corresponding to hafnium as well as strong aluminium and oxygen signals were detected as shown in Figure 3c. To enable detailed analysis of the detection of hafnium and the remaining alumina layer, the central region in Figure 2d was cross-sectioned by FIB milling. The region of interest was widely protected by platinum deposition prior to the milling process and then serially cross-sectioned until identifying any particle or region containing hafnium. The detailed technique of FIB serial milling is described elsewhere [27]. Finally, a tiny particle with different contrast (bright contrast in Figure 2e) was found between the top platinum layer and the base material. The dark contrasting particles are the remaining aluminium oxide. Then, the milling process was stopped, and the region was cleaned using a FIB cleaning process for high resolution and high magnification observation. A highly magnified image in Figure 2f clearly shows that there is a bright particle. Importantly, a SEM-EDX point analysis on the particle clearly shows that there are high amounts of hafnium inside the particle as shown in Figure 3d.

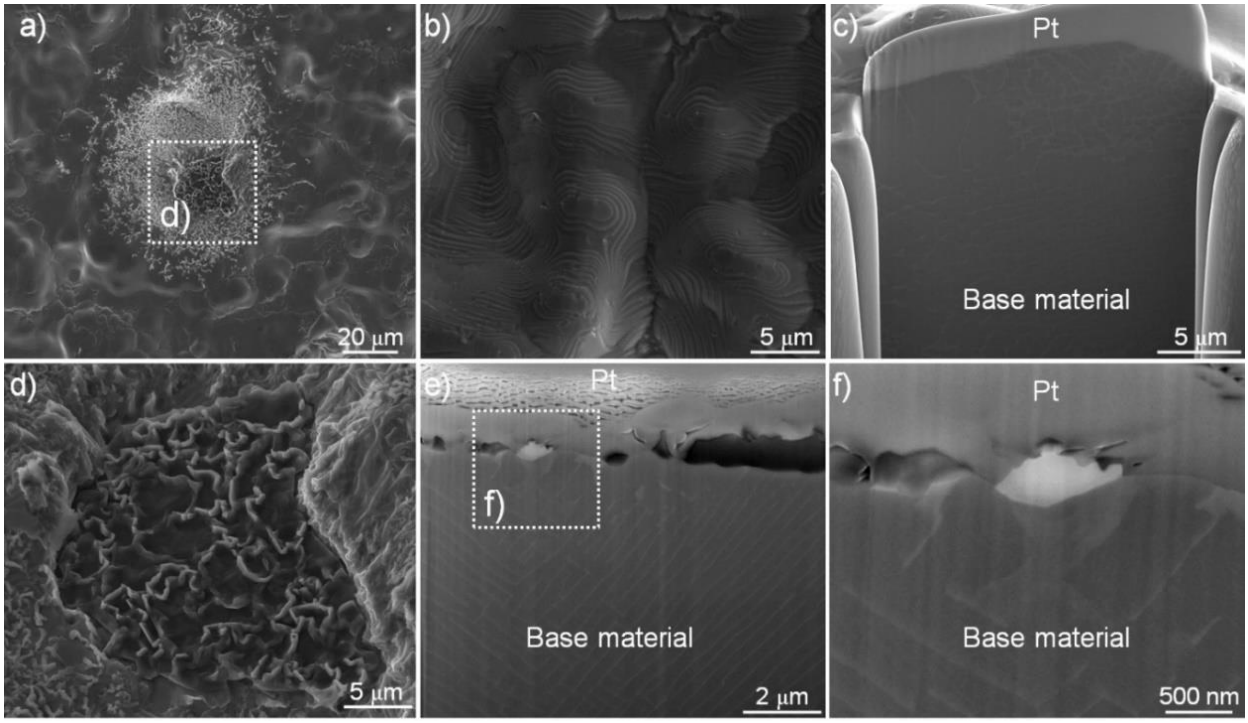


Figure 2. SEM images in a scaled region: (**a**) a low magnification plain view showing an interested region, (**b**,**c**) a magnified plain view image (**b**) and a tilting view image after a FIB milling process (**c**) of a normal area, (**d**) a magnified plain view image at the marked region in panel (**a**), (**e**) a tilting view image near the boundary region in (**d**) after FIB milling, and (**f**) a magnified image at the marked region in (**e**). Note that the surface of interest in (**b**) and (**d**), respectively, was protected by a platinum deposition layer before FIB milling.

Even though a particle containing hafnium was detected and confirmed in Figures 2 and 3, it was necessary to verify this detection in another region or sample because the particle containing hafnium might be an artefact. Another region containing a number of particles within the scaled region was selected as shown in Figure 4a. Except the central region, the morphology is almost the same with the common scaled region in Figure 2b. The region was then cross sectioned by FIB (Figure 4b). Clearly, hafnium signals (which were almost the same with Figure 3c) were acquired from the surface and the cross section, respectively, even though the SEM-EDX point analysis results are not shown in this study. However, TEM observation was performed (see Figure 5). It should be mentioned that whilst there are several particles and layers between the top platinum layer and the base material, it is not a continuous layer (Figure 4b). Before showing detailed observation results, it is necessary to compare the discrete particles shown in Figures 2 and 4 with a normal aluminium oxide layer formed in the same turbine blade. Figure 4c shows a plain view of an unscaled region within the same turbine blade in Figure 1a. For a clear observation without any charging effect during SEM observation, the surface was gold-coated. The surface of an unscaled region (Figure 4c) is completely different from the surface of the scaled region in Figure 2 or Figure 4a. Most of all, the cross section (Figure 4d) clearly shows that there is a continuous layer on the top surface of the base material which is marked with an arrow even though the top surface of the base material is not flat. SEM-EDX analysis on the layer showed almost the same spectrum as Figure 3b and confirmed the layer as aluminium oxide. This means that the discrete layer or particles formed within the scaled region is completely different from the continuous layer formed on the top surface of the unscaled region.

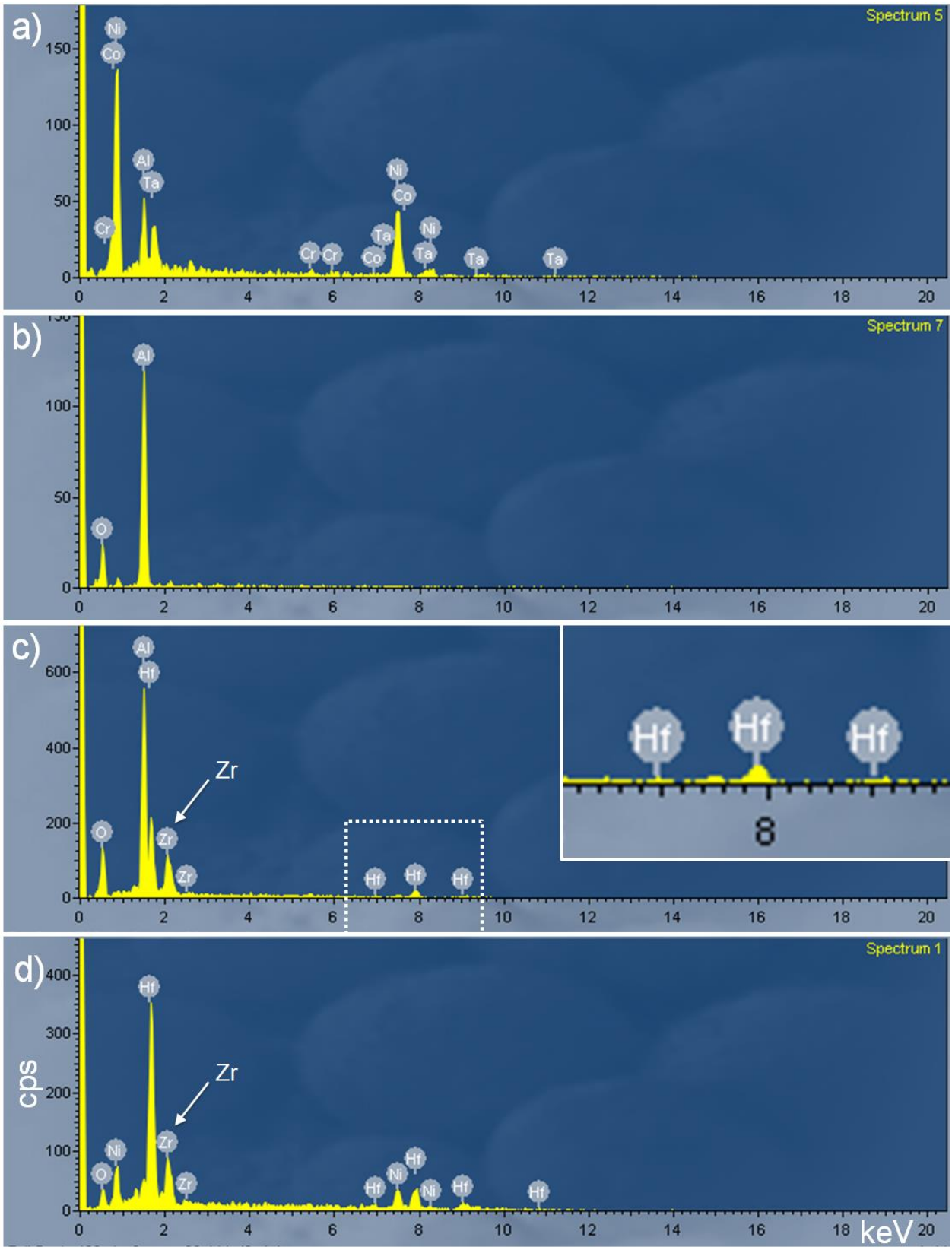


Figure 3. Representative SEM-EDX spectra acquired on a reference base material or metallic particles (**a**), aluminium oxide (**b**), a local area in Figure 2d (**c**), and the tiny particle in Figure 2f (**d**).

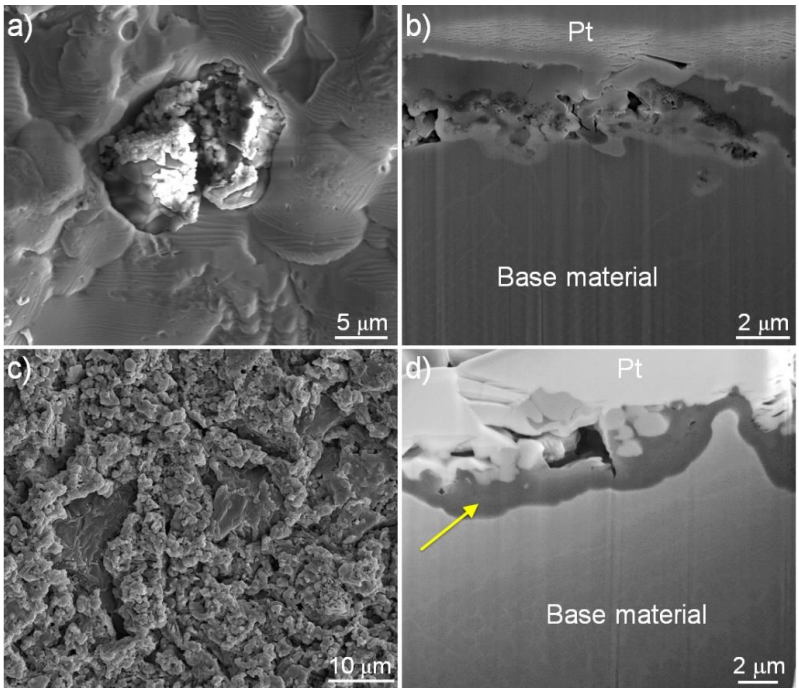


Figure 4. SEM images acquired from a scaled region (**a**,**b**) and an unscaled region (**c**,**d**): (**a**) a plain view of an interested region, (**b**) a tilting view after FIB milling on the central region in (**a**), (**c**) a plain view of an interested region, and (**d**) a tilting view after FIB milling. Note that a platinum layer was deposited on the region of interest in (**a**,**c**), respectively, to protect it during FIM milling, and the surface in (**c**) was gold-coated for conduction during SEM observation.

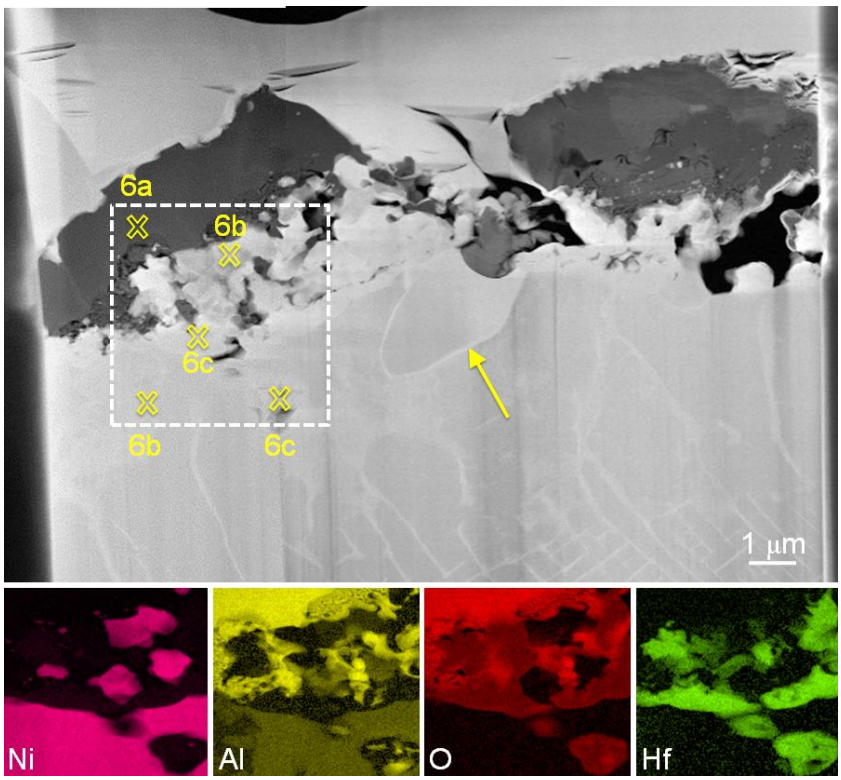


Figure 5. A STEM-HAADF image of the region of interest in Figure 4b after FIB in-situ TEM sampling and STEM-EDX element maps of nickel, aluminium, oxygen, and hafnium in the marked region.

3.2. Detailed Analysis of Particles Containing Hafnium

As shown in Figure 3, SEM-EDX point analysis detected hafnium signals from the surface and the cross section, respectively. However, the interaction volume (with a depth range of a few micrometres) [28–30] of an incident electron beam for SEM-EDX point analysis with the targeting surface of a sample is much larger than the particle size detected in Figures 2f and 4b. In addition, characteristic X-rays (M_α, keV) generated from Hf (1.644), Ta (1.709), W (1.774), and Re (1.842) are extremely close [22,23]. To clearly distinguish each element and enable accurate analysis, a TEM sample was fabricated accurately from the region in Figure 4b using a FIB lift-out technique. Figure 5 shows a TEM image and STEM-EDX element maps. The morphology is the same as that seen in the SEM image of Figure 4b even though the TEM image is mirrored. The top bright layer is platinum, which means that the region of interest was well preserved without any critical damage during FIB milling and cleaning. It should be noted that the bottom base material does not show a normal microstructure of thin γ channels and a fine cuboid γ' phase. Instead, some elongated γ' phase is shown near the top surface of the base material. Between the top protective platinum and the base material, there are several particles with different contrast; it is not a continuous layer. In addition, there are even some pores in this region which display black contrast mainly in the centre-right part. To analyse the elemental distribution in the region of interest, STEM-EDX element maps were acquired at the region marked with a dotted squire in Figure 5. As expected, nickel shows high contrast in the base material. It is clear that nickel also exists in the shape of several particles above the base material. Importantly, there is a region showing an extremely low contrast of nickel inside the base material. Aluminium shows high contrast on the central region, in addition to the outer layer. A STEM-EDX oxygen map shows an interesting distribution and confirms that the top layer and most of the central region are composed of oxides. The element map also indicates clearly that the particle detected inside the base material is an oxide. However, the particles existing above the base material which showed a high contrast of nickel, do not exist as an oxide. It should be also emphasised that the aluminium and the oxygen maps do not match perfectly, especially, inside the base material. In order to understand the distribution of other alloying elements and importantly, to match the elements with the oxygen distribution, STEM-EDX element maps were also acquired for other elements, such as chromium, cobalt, titanium, niobium, molybdenum, tantalum, tungsten, rhenium, and hafnium. Among them, the STEM-EDX hafnium map was completely matched with the remaining oxygen distribution as shown in the figure. Hafnium also shows high contrast inside the base metal, even in areas which showed a low nickel contrast.

For the detailed chemical analysis of the particles found between the top platinum and the base material, a STEM-EDX point analysis was also performed. Figure 6a shows a representative spectrum acquired on the dark contrast particle which is marked as '6a' in Figure 5 just below the platinum layer showed a high contrast of aluminium and oxygen. It contains large amounts of these elements without any other alloying elements or mould material, in particular silicon, which means that the dark contrast particle is purely aluminium oxide. For a reference, a spectrum acquired from the base material which is marked as '6b' in Figure 5 is shown in Figure 6b. The base material shows strong peaks of nickel, cobalt, chromium, and tantalum. It should be noted that a similar STEM-EDX spectra was also acquired from the particles existing above the base material (also marked as another '6b' in Figure 5) which showed high contrast of nickel, which means that they are from the base material. Figure 6c is a representative spectrum acquired from the particle which showed high contrast of hafnium in Figure 5 inside the base material (marked as '6c' in Figure 5), or the particles existing just on the base material (also marked as another '6c' in Figure 5). There are strong peaks corresponding to hafnium and oxygen, which means that the particles are hafnium oxide. It should be noted that in the spectrum, there are also some additional peaks at 2.04 keV and 15. 74 keV. Near 2.04 keV, there are several candidates such as phosphorus (K_α, 2.01 keV), zirconium (L_α, 2.04 keV), and platinum (M_α, 2.05 keV) [22,31]. However, also considering the energy peak acquired at 15.74 keV as

well as potential elements involved the casting process, the corresponding candidate is just zirconium (K_α, 15. 74 keV). This means that the hafnium oxide also contains zirconium. As shown in the inserts in Figure 6, the zirconium signal was not detected in any other particle or region. It should be noted that comparing STEM-EDX spectra (Figure 6) with SEM-EDX ones (Figure 3), even SEM-EDX point analysis could detect zirconium with hafnium, which means that every hafnium oxide in this study contained zirconium. Most of all, even SEM-EDX could be used to detect zirconium in the hafnium oxide.

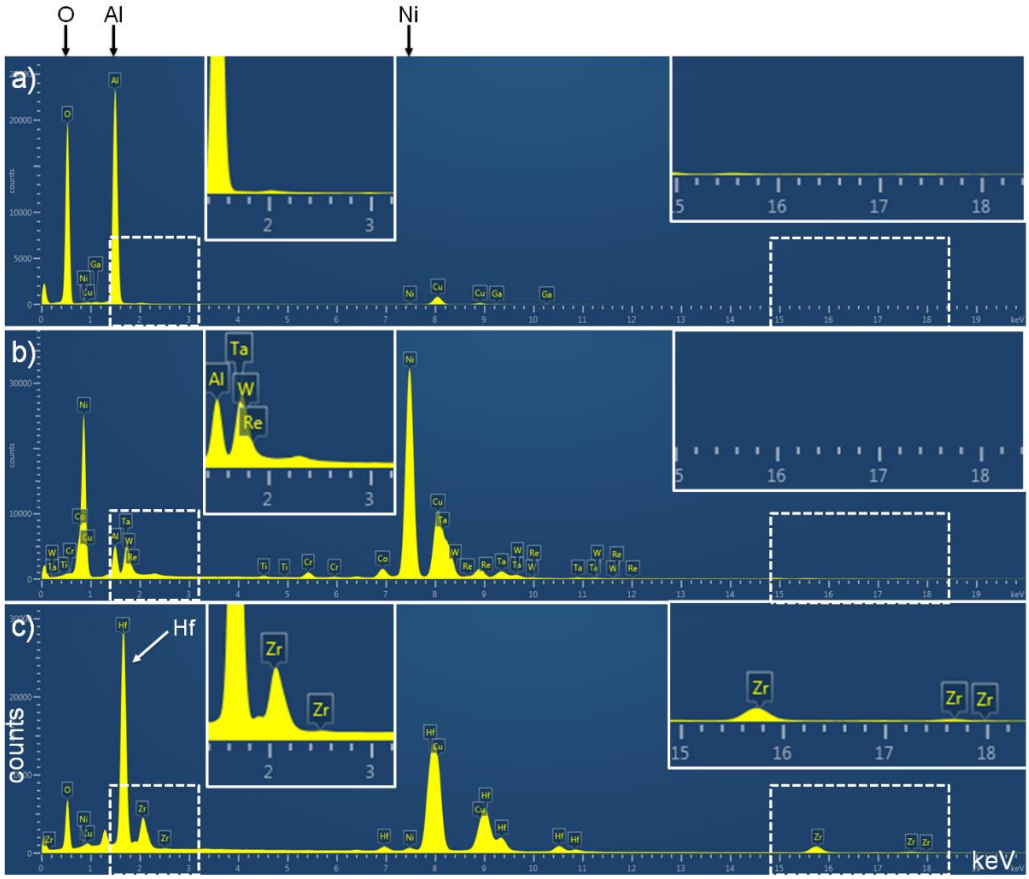


Figure 6. Representative STEM-EDX spectra acquired on aluminium oxide (**a**), a base material or small particles (**b**), and hafnium oxide (**c**). For clear visualisation of key energy ranges, two regions in a spectrum, respectively, were magnified and added as inserts.

Based on the STEM-EDX point analysis, the compositions of the base material and oxides were summarised in Table 1 and compared with those acquired from as-manufactured turbine blades which were fully heat-treated by well-established solution and aging processes [24–26]. Even though the amount of hafnium in the base material or fully heat-treated γ and γ' phases is insignificant, the amount in the hafnium oxide is extremely high. This means that even the negligible amounts of hafnium in the raw material were probably almost consumed by the formation of the hafnium oxide near the top surface of the base material. It should be noted that the outer surface of as-cast turbine blades is usually removed by post-processing, such as blasting and grinding, in the foundry. As a result, the amount of hafnium inside the base material after the manufacturing process is extremely low or non-existent, and it is therefore difficult to find any hafnium within a fully heat-treated turbine blade. Table 1 also shows the composition of the base material based on the spectrum in Figure 6b. Though the morphology of the base material looked like a γ' phase near the top surface as shown in Figures 2, 4 and 5, its composition was quite different from those of γ and γ' phases in fully heat-treated turbine blades. The amount of aluminium, which is the main forming element for the γ' phase, is much lower in the

base material because large amounts of aluminium near the top surface of the base material were consumed in the formation of the aluminium oxide, which will be discussed later. In contrast, just a small amount of hafnium was detected. During post-processing such as solution and aging heat treatment, aluminium atoms can diffuse from the internal base material and then a γ' phase with the typical aluminium composition can be formed.

Figure 5 clearly showed a hafnium oxide near the top surface of the base material. It should be noted that there is also one particle showing a different morphology which is marked with an arrow in Figure 5. Even though the detailed analysis of the particle is beyond the scope of this study (see Refs. [32,33]), it is appropriate to show the analysis to allow better understanding of the formation mechanism of the scaled region and the hafnium oxide containing zirconium. Figure 7 shows a STEM-HAADF image and STEM-EDX analyses of the particle. The particle is slightly brighter than the base material, which means that the particle may contain heavier elements than nickel (Figure 7a). However, the corresponding STEM-EDX oxygen map indicates that the particle is not an oxide. Of STEM-EDX element maps of alloying elements, a STEM-EDX rhenium map (Figure 7a) was well matched with the region. Most of all, a STEM-EDX point analysis (Figure 7b) on the particle clearly shows high energy peaks corresponding to rhenium. The composition summarised in Table 1 indicates that the particle contains large amounts of rhenium as well as chromium and tungsten. The detection of the rhenium-rich particle on the top surface of the base material in the scaled region is important to understand the formation of the surface scale as well as the hafnium oxide, which will be discussed later.

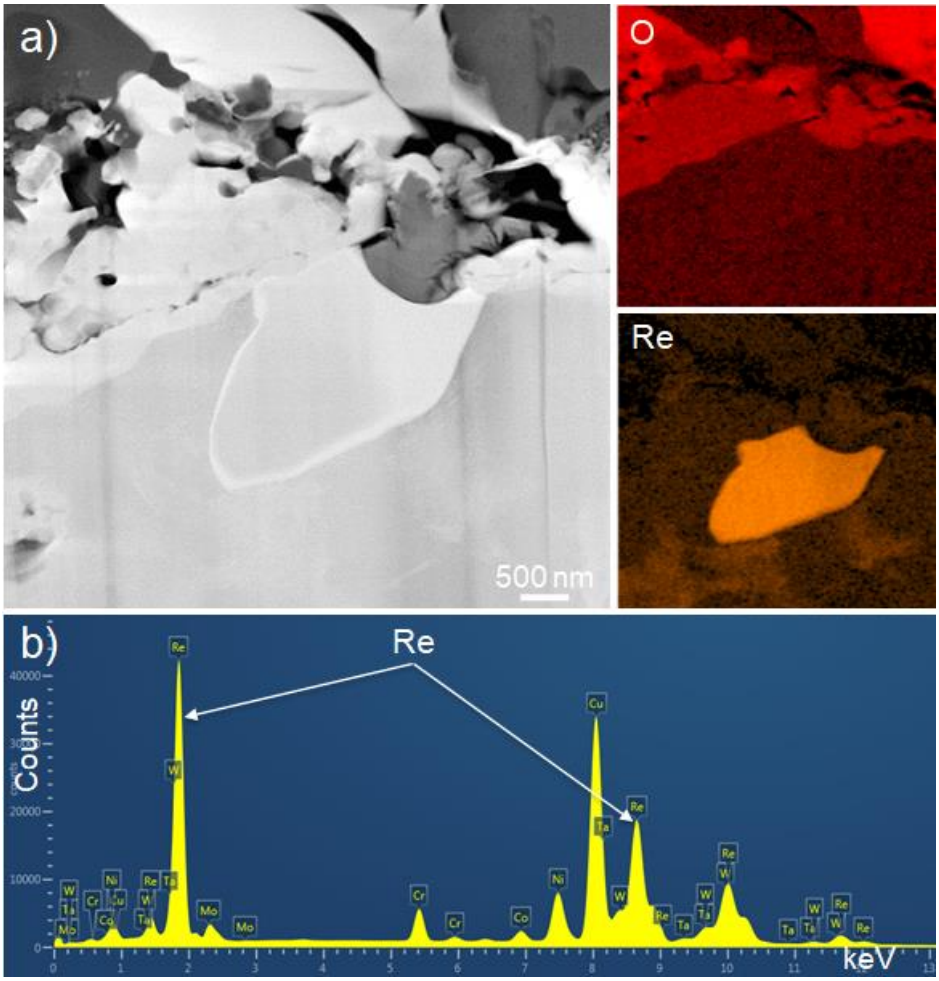


Figure 7. A STEM image and corresponding STEM-EDX element maps of oxygen and rhenium (**a**) and STEM-EDX point analysis on the bright particle in (**a**,**b**).

4. Discussion

4.1. Formation of the Scaled Region

As already shown recently by the authors [15], during casting, there is a strong interaction between the mould wall which is composed of a ceramic slurry of a silica sol with zirconium silicate flour and the superalloy melt which contains aluminium. As a result, aluminium oxide forms on the surface of a casting turbine blade by the following reaction when the melt is in contact with the mould:

$$\frac{2}{3}\mathrm{Al} + \frac{1}{2}\mathrm{SiO_2} \rightarrow \frac{1}{3}\mathrm{Al_2O_3} + \frac{1}{2}\mathrm{Si}$$

As shown in Table 2 [34], the change in Gibbs free energy (ΔG_f) for the reaction at 1800 K (1527 °C) is −70.955 kJ/mol, which means that this reaction is spontaneous. Then, the aluminium oxide covers the whole surface of the casting blade.

Table 2. Possible chemical reactions and the change in Gibbs free energy at 1800 K (1527 °C) based on thermochemical data [34].

Reactions	ΔG_f (at 1800 K, kJ/mol)
$\frac{1}{2}\mathrm{Si} + \frac{1}{2}\mathrm{O_2} \rightarrow \frac{1}{2}\mathrm{SiO_2}$	−295.189
$\frac{2}{3}\mathrm{Al} + \frac{1}{2}\mathrm{O_2} \rightarrow \frac{1}{3}\mathrm{Al_2O_3}$	−366.144
$\frac{1}{2}\mathrm{Hf} + \frac{1}{2}\mathrm{O_2} \rightarrow \frac{1}{2}\mathrm{HfO_2}$	−412.522
$\frac{2}{3}\mathrm{Cr} + \frac{1}{2}\mathrm{O_2} \rightarrow \frac{1}{3}\mathrm{Cr_2O_3}$	−225.242
$\frac{1}{2}\mathrm{Zr} + \frac{1}{2}\mathrm{O_2} \rightarrow \frac{1}{2}\mathrm{ZrO_2}$	−381.782
$\frac{1}{4}\mathrm{Zr} + \frac{1}{4}\mathrm{Si} + \frac{1}{2}\mathrm{O_2} \rightarrow \frac{1}{4}\mathrm{ZrSiO_4}$	−337.389
$\frac{2}{3}\mathrm{Al} + \frac{1}{2}\mathrm{SiO_2} \rightarrow \frac{1}{3}\mathrm{Al_2O_3} + \frac{1}{2}\mathrm{Si}$	−70.955
$\frac{1}{2}\mathrm{Hf} + \frac{1}{2}\mathrm{ZrO_2} \rightarrow \frac{1}{2}\mathrm{HfO_2} + \frac{1}{2}\mathrm{Zr}$	−30.740
$\frac{1}{2}\mathrm{Hf} + \frac{1}{3}\mathrm{Al_2O_3} \rightarrow \frac{1}{2}\mathrm{HfO_2} + \frac{2}{3}\mathrm{Al}$	−46.378
$\frac{1}{2}\mathrm{Hf} + \frac{1}{2}\mathrm{SiO_2} \rightarrow \frac{1}{2}\mathrm{HfO_2} + \frac{1}{2}\mathrm{Si}$	−117.333
$\frac{1}{2}\mathrm{Hf} + \frac{1}{4}\mathrm{ZrSiO_4} \rightarrow \frac{1}{2}\mathrm{HfO_2} + \frac{1}{4}\mathrm{Zr} + \frac{1}{4}\mathrm{Si}$	−75.134

During cooling of cast components, different thermal expansion coefficients of the ceramic mould and the metallic blade induce different contractions and as a result, the casting component becomes detached from the mould. The spallation usually occurs near the interface of the aluminium oxide layer and the mould wall. However, a previous study showed that aluminium silicate could form on the surface of a casting turbine blade due to the reaction of aluminium and silica at high temperature [35]. Furthermore, even though rhenium has the slowest diffusion rate (the diffusion coefficient of 8×10^{-17} m^2 s^{-1} at 1300 °C) of all the alloying elements in the Ni-based superalloys [36], rhenium-rich particles could also be found in this region as shown in Figure 7. This means that some areas within a turbine blade are probably exposed to a high temperature for a sufficient period to form the aluminium silicate and to induce diffusion of rhenium atoms to form rhenium-rich particles. In this region, the aluminium oxide layer contacting silica may not be stable in these conditions. Consequently, the aluminium oxide is no longer a continuous layer through the reaction with silica, and as a result of this, it cannot completely cover the top surface of the base material. When the spallation occurs in the area within a turbine blade, such as the aerofoil where the hottest casting temperatures are held for longest, the detachment can happen at the interface of the broken aluminium oxide or the aluminium silicate and the base material due to their relatively weak bond. As a result, a fresh surface of the base material is exposed, which is the silver-scaled region in this study. However, in the unscaled region, the continuous aluminium oxide layer remains.

It should be noted that regardless of the scaled or the unscaled region, the cross sections of the base material in Figures 2 and 4 do not show a normal microstructure (which is composed of thin γ channels and a fine and uniform γ' phase) because the turbine blade is an as-cast state. The expected microstructure is produced through post-casting of solution heat treatment and aging.

4.2. Formation of Hafnium Oxide Containing Zirconium on the Surface of a Scaled Region

An aluminium oxide layer forms on the top surface of the base material through the reaction of aluminium and silicon oxide. However, as shown in this study, hafnium oxide containing zirconium also exists between the aluminium oxide and the base material within the scaled region. Zirconium can come only from the ceramic mould materials if there is no other source. The formation mechanism of the hafnium oxide containing zirconium is probably complicated due to the number of alloying elements and the nature of the casting process. Before discussing the detailed mechanism, three facts must be highlighted:

1. That the solubility of hafnium in γ and γ' phases is low;
2. That the concentration of hafnium is extremely low in the raw material;
3. That the scaled region where the hafnium oxide is usually detected, solidifies late in the process.

4.2.1. Possibility of Formation of Hafnium Oxide by the Diffusion of Hafnium and Zirconium

The formation mechanism of hafnium oxide containing zirconium is probably explained by the diffusion of hafnium and zirconium. During solidification, hafnium segregates into the interdendritic regions due to its low solubility in both the γ and γ' phases [2,37]. Then, for the observed microstructure in this study, as the interdendritic regions are composed of an abnormal microstructure of γ and γ' phases, hafnium atoms should diffuse onto the surface through γ or γ' phases although its solubility is low in those phases. It should be noted that there are a higher volume of γ' phase in the interdendritic region, but the diffusion activity energy of hafnium in γ' is higher than that in γ due to the ordered structure [38]. Therefore, the diffusion of hafnium through the γ' phase may not be sufficient to occur during casting. However, at high temperatures such as casting temperature, the heat activation makes more vacancies of aluminium atoms in γ' and the degree of ordering in γ' decreases [38]. In addition to this, the diffusion energy barrier of hafnium is much lower than any other alloying elements, and the value is the lowest in the 5d transition metals (three or four times lower than that of tungsten or rhenium) [1,36]. Hence, hafnium atoms may be able to diffuse onto the surface during casting. As hafnium is added to directionally solidified nickel-based superalloys to strengthen grain boundaries, the migration to the surface of a single crystal casting is consistent with this.

There is then an opportunity for hafnium to form an oxide either through reaction with oxygen or by a reduction/oxidation reaction with other oxides. As the melt is inside the mould in vacuum during casting, there is probably just a possibility to react with other oxides, such as the already-formed aluminium oxide or the mould wall materials composed of oxides. As shown in Table 2, the reaction of hafnium and the aluminium oxide is thermodynamically spontaneous, which means that the reaction is favourable. However, it should be emphasised that as already shown in the previous section, the hafnium oxide formed on the top surface of the base material contains zirconium, but it does not contain aluminium, which means that zirconium should diffuse onto the hafnium oxide from the mould wall because there is only one source of zirconium in the casting process. Zirconium atoms in a mould wall material may diffuse through the aluminium oxide and pile up into the hafnium oxide. However, the aluminium oxide formed at the casting temperature of about 1500 °C is a highly stable and continuous α-Al_2O_3 phase with a hexagonal close-packed structure, and most of all, the oxide is almost free from cracks or pores [12,18]. Therefore, considering the atomic size and the possibility of diffusion of zirconium in atomic scale through α-Al_2O_3, it is almost impossible for the diffusion of zirconium through the aluminium oxide to occur. Most of all, within the aluminium oxide, no signal of zirconium or gradual concentration decrease in zirconium through the aluminium oxide was seen, as shown in Figures 3b and 6a. In addition, as the reaction of hafnium and the aluminium oxide might occur through the whole top surface of a turbine blade, the hafnium oxide should have also been detected in the unscaled region (not in only the scaled region) if the reaction occurred. Therefore, even though it is thermodynamically

possible for the reaction of hafnium with the aluminium oxide to occur, the detection of zirconium in the hafnium oxide and no detection of zirconium in the aluminium oxide or no detection of hafnium oxide in the unscaled region cannot be simply explained by the reaction and the diffusion of hafnium and zirconium.

4.2.2. Possibility of a Reaction of Hafnium with Mould Wall Materials

There is another possibility to form hafnium oxide containing zirconium through a direct reaction of hafnium with ceramic mould materials. During casting, the so-called 'Primary Coat' of a ceramic mould, which is a mixture of 18% silicon oxide and 82% zirconium silicate, contacts the molten base material [8]. Therefore, hafnium near the top surface of the base material may meet and react with silicon oxide or zirconium silicate in the mould by the following reaction:

$$\frac{1}{2}\mathrm{Hf} + \frac{1}{2}\mathrm{SiO_2} \rightarrow \frac{1}{2}\mathrm{HfO_2} + \frac{1}{2}\mathrm{Si}$$

or

$$\frac{1}{2}\mathrm{Hf} + \frac{1}{4}\mathrm{ZrSiO_4} \rightarrow \frac{1}{2}\mathrm{HfO_2} + \frac{1}{4}\mathrm{Zr} + \frac{1}{4}\mathrm{Si}$$

For the reactions, the changes in ΔG_f at 1800 K (1527 °C) are −117.333 kJ/mol and −75.134, respectively, as shown in Table 2. These ΔG_f changes for the reaction of hafnium with the ceramic mould wall materials are much lower than any other elements in the base material. As a result, hafnium can easily form its oxide if it contacts with the mould material.

Compared with aluminium in the molten material, the amounts of hafnium are extremely too low to cover the whole surface of a turbine blade. As a result, depending on the sampling locations, hafnium oxide might be locally detected. However, as already mentioned, it is well known that aluminium oxide is formed by the reaction of aluminium in the melt and silicon oxide in the mould, and it covers the whole surface of the melt, which means that the already-formed aluminium oxide can prevent hafnium meeting the mould wall materials. In addition, as the concentration of hafnium in the melt is extremely low, the formation of hafnium oxide is limited or it may occur extremely locally. This means that the aforementioned reaction of aluminium in the melt and silicon oxide in the mould is the predominant reaction. The byproduct (aluminium oxide) covers the top surface of the melt, and consequently, the reaction of hafnium with the mould cannot explain the detection of hafnium oxide in the scaled region.

4.2.3. Formation of Hafnium Oxide Containing Zirconium

The diffusion of hafnium and zirconium or the direct reaction of hafnium with mould wall materials was not sufficient to explain the formation of hafnium oxide containing zirconium mainly due to the existence of the aluminium oxide formed on the top surface of the base material. However, even though the surface of the melt is covered with an aluminium oxide, if the oxide is broken, hafnium in the melt can meet the mould materials and may form relatively easily the hafnium oxide with zirconium. Before discussing another possibility, it is necessary to mention that, as shown in Figures 2, 4 and 5, hafnium oxide containing zirconium was detected near or beneath the aluminium oxide where this was not a continuous layer. In addition, a previous study on similar turbine blades with the surface scale clearly showed aluminium silicate particles over the aluminium oxide or even near the base material [15]. This means that the aluminium oxide can react with silicon oxide which is one of main materials of the ceramic mould and as a result, the continuous aluminium oxide layer can be broken as shown in Figures 2, 4 and 5.

Then, as the aluminium oxide is not continuous, there is a possibility that hafnium near the top surface of the base material can meet and react with silicon oxide or zirconium silicate in the mould. During solidification, hafnium is pushed onto the tips of dendrite arms due to its low solubility in both the γ and γ' phases. As a result, hafnium is segregated

to the late solidifying part in the casting component, i.e., the aerofoil part of a turbine blade which is the scaled region in this study. As the concentration of hafnium is focused on this region, more hafnium can react even with the already-formed aluminium oxide, and most of all, with the mould wall materials, in particular, zirconium silicate. Consequently, they can form hafnium oxide just in the late solidifying aerofoil part of a turbine blade. Considering the composition of hafnium oxide and the detection of zirconium without silicon (Table 1), it appears that when hafnium reacts with zirconium silicate, a small amount of zirconium may remain inside the oxide as a solute due to the nearly identical chemical properties of hafnium and zirconium [39]. As a result, hafnium oxide contains a small amount of zirconium.

4.3. Meaning of the Detection of Hafnium Oxide Containing Zirconium on the Surface of a Scaled Region

The detection of hafnium oxide containing zirconium as well as a rhenium-rich particle in the scaled region definitely supported the formation mechanism of surface scale, even though the oxide and the particle did not directly show any effect on the formation of surface scale in this study. The detection confirmed that the surface scaled region could be exposed to high enough temperatures to allow the diffusion of heavy alloying elements, such as hafnium and rhenium. In addition, the formation of hafnium oxide with zirconium proved that the molten base material could react with the mould wall materials like the formation of an aluminium oxide by the reaction of aluminium in melt and silica in the mould. This means that to prevent the reaction, it may require the development of new face coat materials that contact to the melt.

Furthermore, the detection of hafnium oxide indicated that most of hafnium in the scaled region might be consumed by the formation of its oxide. Hafnium is one of the minor alloying elements in third generation single crystal turbine blades even though the concentration is not high. However, as shown in this study, if the surface scale is formed, hafnium can be consumed by the formation of its oxide. Consequently, it is unlikely that hafnium in a turbine blade, especially containing a surface scale defect, can contribute to the formation of a normal microstructure composed of thin γ channels and a precipitate of γ'. In addition, as single crystal turbine blades do not have any grain boundary, hafnium has no effect as a grain boundary strengthening element for their mechanical properties and environmental resistance. Therefore, this study suggests that the optimum amounts of hafnium are much lower than the current value even though the amounts are already low, or it may not even be necessary to add hafnium any longer. Importantly, it can contribute to simplifying the complexity of the manufacturing process of Ni-based single crystal superalloy turbine blades—one of the most complicated materials which contain a number of alloying elements and experience a number of metallurgical phenomena during the manufacturing process. Based on this study, it may be necessary to investigate the actual effect of any other minor alloying elements in the turbine blades. Furthermore, as rhenium—which accounts for 80% of total alloy cost—can be also consumed by the formation of undesired rhenium-rich particles, further research on optimum amounts of each element or prevention of the formation of undesired particles may be required.

5. Summary

A turbine blade containing surface scale was removed from the manufacturing runner system and observed by electron microscopy. The scaled region was easily recognised due to its different contrast on the surface. SEM images showed that the surface of the scaled region was dimpled, but no specific morphology was observed at low magnifications. However, higher magnification observation of the scaled region revealed a smooth surface and flat terrain of steps slightly protruding from the surface. Furthermore, in the scaled region, several fine particles including hafnium oxide were detected without any continuous aluminium oxide layer. High resolution TEM analysis on the oxide showed some peaks corresponding to zirconium. However, any energy peak of zirconium was not

detected in any other particle, oxide, or the base material. By comparison, in the unscaled region, a continuous aluminium oxide layer covered the top surface. This study suggested that even though it was well known that a continuous aluminium oxide layer was initially formed by the reaction of aluminium in the melt with silicon oxide in the ceramic mould, there was a possibility that the aluminium oxide layer was broken, and then, hafnium in the base material could react with silicon oxide and/or zirconium silicate as well as with the aluminium oxide and form hafnium oxide between the aluminium oxide and the base. In addition, due to the nearly identical chemical properties of hafnium and zirconium, hafnium oxide after casting might inevitably contain zirconium as shown in this study.

Author Contributions: Conceptualization, development of the methodology, and analysis of the data was performed by K.P.; discussion was performed by K.P. and P.W.; writing and review was performed by K.P. and P.W. All authors have read and agreed to the published version of the manuscript.

Funding: This work was supported by the Engineering and Physical Sciences Research Council, grant number EP/T018518/1.

Acknowledgments: The financial support and provision of evaluation test pieces by Rolls-Royce plc is acknowledged.

Conflicts of Interest: The authors declare no conflict of interest.

References

1. Reed, R.C. *The Superalloys: Fundamentals and Applications*; Cambridge University Press: Cambridge, UK, 2006; pp. 33–86.
2. Geddes, B.; Leon, H.; Huang, X. *Superalloys: Alloying and Performance*; ASM International: Materials Park, OH, USA, 2010; pp. 1–109.
3. Durand-Charre, M. *The Microstructure of Superalloys*; OPA: Amsterdam, The Netherlands, 1997; pp. 1–12.
4. Bar-Cohen, Y. *High Temperature Materials and Mechanisms*; CRC Press: Boca Raton, FL, USA, 2014; pp. 110–117.
5. Kotval, P.S.; Venables, J.D.; Calder, R.W. The role of hafnium in modifying the microstructure of cast nickel-base superalloys. *Metall. Mater. Trans. B* **1972**, *3*, 457–462. [CrossRef]
6. Amouyal, Y.; Seidman, D.N. The role of hafnium in the formation of misoriented defects in Ni-based superalloys: An atom-probe tomographic study. *Acta Mater.* **2011**, *59*, 3321–3333. [CrossRef]
7. Hou, J.S.; Guo, J.T.; Wu, Y.X.; Zhou, L.Z.; Ye, H.Q. Effect of hafnium on creep behavior of a corrosion resistant nickel base superalloy. *Mater. Sci. Eng. A* **2010**, *527*, 1548–1554. [CrossRef]
8. Brewster, G.; D'Souza, N.; Ryder, K.S.; Simmonds, S.; Dong, H.B. Mechanism for Formation of Surface Scale during Directional Solidification of Ni-Base Superalloys. *Metall. Mater. Trans. A* **2012**, *43*, 1288–1302. [CrossRef]
9. Panwisawas, C.; Mathur, H.; Gebelin, J.C.; Putman, D.; Rae, C.M.F.; Reed, R.C. Prediction of recrystallization in investment cast single-crystal superalloys. *Acta Mater.* **2013**, *61*, 51–66. [CrossRef]
10. Mathur, H.N.; Panwisawas, C.; Jones, C.N.; Reed, R.C.; Rae, C.M.F. Nucleation of recrystallisation in castings of single crystal Ni-based superalloys. *Acta Mater.* **2017**, *129*, 112–123. [CrossRef]
11. Brewster, G.; Dong, H.B.; Green, N.R.; D'Souza, N. Surface Segregation during Directional Solidification of Ni-Base Superalloys. *Metall. Mater. Trans. B* **2008**, *39*, 87–93. [CrossRef]
12. Prescott, R.; Graham, M.J. The formation of aluminum oxide scales on high-temperature alloys. *Oxid. Met.* **1992**, *38*, 233–254. [CrossRef]
13. Simmonds, S.; Souza, N.D.; Ryder, K.S.; Dong, H. Analysis of surface scale on the Ni-based superalloy CMSX-10N and proposed mechanism of formation. *IOP Conf. Series: Mater. Sci. Eng.* **2012**, *27*, 012038. [CrossRef]
14. Ul-Hamid, A. TEM Study of Scale Microstructures Formed on Ni–10Cr and Ni–10Cr–5Al Alloys with and Without Y Addition. *Oxid. Met.* **2002**, *58*, 41–56. [CrossRef]
15. Park, K.; Withey, P. Formation and Prevention of a Surface Defect on the Aerofoil of As-Cast Nickel-Based Single-Crystal Turbine Blades. *Adv. Eng. Mater.* **2021**, *23*, 2100302. [CrossRef]
16. Park, K.; Withey, P. Formation of Secondary Phases in the Boundary between Surface Defect Grains and Matrix in Third Generation Nickel-Based Single Crystal Superalloy Turbine Blades. In *Thermec 2018: 10th International Conference on Processing and Manufacturing of Advanced Materials*; Shabadi, R., Ionescu, M., Jeandin, M., Richard, C., Chandra, T., Eds.; Trans Tech Publications: Bäch, Switzerland, 2018; Volume 941, pp. 766–771.
17. Kim, K.; Watanabe, M.; Kawakita, J.; Kuroda, S. Grain refinement in a single titanium powder particle impacted at high velocity. *Scripta Mater.* **2008**, *59*, 768–771. [CrossRef]
18. Kim, K. Formation of Fine Clusters in High-Temperature Oxidation of Molten Aluminum. *Metall. Mater. Trans. A* **2014**, *45*, 3650–3660. [CrossRef]
19. Kim, K.; Watanabe, M.; Kuroda, S.; Kawano, N. Observation of high resolution microstructures in thermal sprayed coatings and single deposited splats using ion beam milling. *Mater. Trans.* **2011**, *52*, 439–446. [CrossRef]

20. Kim, K.; Watanabe, M.; Kawakita, J.; Kuroda, S. Effects of Temperature of In-flight Particles on Bonding and Microstructure in Warm-Sprayed Titanium Deposits. *J. Therm. Spray Tech.* **2009**, *18*, 392–400. [CrossRef]
21. Kim, K.; Withey, P. Formation of an Intermediate Layer Between Grains in Nickel-Based Superalloy Turbine Blades. *Metall. Mater. Trans. A* **2017**, *48*, 2932–2942. [CrossRef]
22. JEOL-Energy Table for EDS Analysis. Available online: www.jeol.com (accessed on 28 September 2013).
23. Warren, P.J.; Cerezo, A.; Smith, G.D.W. An atom probe study of the distribution of rhenium in a nickel-based superalloy. *Mater. Sci. Eng. A* **1998**, *250*, 88–92. [CrossRef]
24. Erickson, G.L. The development and application of CMSX (R)-10. In *Superalloys 1996*; Kissinger, R.D., Deye, D.J., Anton, D.L., Cetel, A.D., Nathal, M.V., Pollock, T.M., Woodford, D.A., Eds.; Minerals, Metals & Materials Society: Pittsburgh, PA, USA, 1996; pp. 35–44.
25. Kim, K.; Withey, P.; Griffiths, W.D. Detection of an Intermediate Layer Containing a Rhenium-Rich Particle at Grain Boundaries Formed Within Single Crystal Nickel-Based Superalloys. *Metall. Mater. Trans. A* **2015**, *46*, 1024–1029. [CrossRef]
26. Kim, K.; Withey, P. Microstructural Investigation of the Formation and Development of Topologically Close-Packed Phases in a 3rd Generation Nickel-Base Single Crystal Superalloy. *Adv. Eng. Mater.* **2017**, *19*, 1700041. [CrossRef]
27. Kim, K. FIB serial milling and lifting out of fine inclusions in an intensively melt sheared aluminum alloy. *Mater. Lett.* **2014**, *117*, 74–77. [CrossRef]
28. Shimizu, R.; Ze-Jun, D. Monte Carlo modelling of electron-solid interactions. *Rep. Prog. Phys.* **1992**, *55*, 487–531. [CrossRef]
29. Demers, H.; Poirier-Demers, N.; Couture, A.R.; Joly, D.; Guilmain, M.; de Jonge, N.; Drouin, D. Three-dimensional electron microscopy simulation with the CASINO Monte Carlo software. *Scanning* **2011**, *33*, 135–146. [CrossRef]
30. Park, K.; Withey, P. Compositions of Gamma and Gamma Prime Phases in an As-Cast Nickel-Based Single Crystal Superalloy Turbine Blade. *Crystals* **2022**, *12*, 299. [CrossRef]
31. Yvon, H.J. Table of X-ray Emission Lines. Available online: www.horiba.com (accessed on 28 September 2022).
32. Kim, K.; Withey, P. Detection of Rhenium-Rich Particles at Grain Boundaries in Nickel-Base Superalloy Turbine Blades. *Mater. Trans.* **2016**, *57*, 1698–1706. [CrossRef]
33. Kim, K.; Withey, P. General View of Rhenium-Rich Particles along Defect Grain Boundaries Formed in Nickel-Based Single-Crystal Superalloy Turbine Blades: Formation, Dissolution and Comparison with Other Phases. *Crystals* **2021**, *11*, 1201.
34. Barin, I. *Thermochemical Data of Pure Substances*; Wiley-VCH: New York, NY, USA, 1995.
35. Duval, J.D.; Risbud, S.H.; Shackelford, J.F. Mullite. In *Ceramic and Glass Materials*; Shackelford, J., Doremus, R.H., Robert, H., Eds.; Springer: New York, NY, USA, 2008; pp. 27–39.
36. Janotti, A.; Krčmar, M.; Fu, C.L.; Reed, R.C. Solute Diffusion in Metals: Larger Atoms Can Move Faster. *Phys. Rev. Lett.* **2004**, *92*, 085901. [CrossRef] [PubMed]
37. Holt, R.T.; Wallace, W. Impurities and trace elements in nickel-base superalloys. *Int. Met. Rev.* **1976**, *21*, 1–24. [CrossRef]
38. Shuwei, M.; Yunrong, Z. Diffusion behaviour of hafnium in Ni and Ni3Al. *J. Mater. Sci. Lett.* **1997**, *16*, 1761–1763. [CrossRef]
39. Takeda, O.; Uda, T.; Okabe, T.H. Rare Earth, Titanium Group Metals, and Reactive Metals Production. In *Treatise on Process Metallurgy*; Seetharaman, S., Ed.; Elsevier: Boston, MA, USA, 2014; pp. 995–1069.

Disclaimer/Publisher's Note: The statements, opinions and data contained in all publications are solely those of the individual author(s) and contributor(s) and not of MDPI and/or the editor(s). MDPI and/or the editor(s) disclaim responsibility for any injury to people or property resulting from any ideas, methods, instructions or products referred to in the content.